JOURNAL OF PROPULSION AND POWER
Vol. 12, No. 1, January–February 1996

Electric Probe Measurements in the Plume of an Ion Thruster

P. C. T. de Boer*
The Aerospace Corporation, Los Angeles, California 90009-2957

Results are presented of measurements with double and single electric probes in the beam of a UK-10 ion thruster, using xenon as the propellant gas. The probe material consisted of tungsten and secondary emission was of negligible importance. As a consequence of the large directed velocity of the ions, the ion current to a probe was essentially independent of probe voltage. Since the debye length was small compared with the probe radius, no ions or electrons were collected on the downstream part of a probe. The thruster was operated at a thrust level of 18 ± 0.3 mN. Detailed results are given for ion flux profiles and ion density in the beam, as well as for floating potential profiles and degree of nonneutralization. Ion densities reach a maximum of 1.8 ± 0.2 × 10^{10} cm^{-3} on the beam centerline at an axial distance of 15 ± 0.3 cm from the acceleration grid. The floating potential at that location is 8.5 ± 0.2 V with respect to the neutralizer, while the degree of nonneutralization there is on the order of 10^{-4}. Characteristic electron energies vary from 0.5 to 2.7 eV. Evidence is obtained that the electron gas has a non-Maxwellian speed distribution function.

Nomenclature

D = diameter of probe
E_i = ion energy
e = electron charge
g = speed distribution function
J = current
$\bar{J}$ = nondimensional current
J_{sat} = $\alpha e n_i u_i D L$, saturation current
j = current density
k = Boltzmann constant
L = length of probe
m = mass
n = number density
r = radius
T = temperature
u = directed velocity, drift velocity
V = electric potential
V_d = potential difference applied to double probe
V_f = floating potential of probe
V_{pl} = plasma potential
v = thermal speed
α = secondary emission coefficient
ε_0 = dielectric constant for vacuum
η = $-eV/kT_e$, nondimensional potential
λ_D = $(\varepsilon_0 kT_e/n_{e0}e^2)^{1/2}$, debye length
ρ = r/λ_D
ϕ_d = eV_d/kT_e, nondimensional potential of double probe

Subscripts
e = electron
i = ion
m = maximum
pr = probe
s = sheath
0 = undisturbed plasma
1, 2 = components of double probe

Received April 22, 1994; revision received Nov. 17, 1994; accepted for publication June 11, 1995.

*Research Physicist, P.O. Box 92957; currently Professor, Sibley School of Mechanical and Aerospace Engineering, Upson Hall, Cornell University, Ithaca, NY 14853. Associate Fellow AIAA.

I. Introduction

THE use of electric probes is a common diagnostic technique for analyzing plasmas. Measurements using such probes are very simple; all that is needed is a suitably mounted thin wire serving as the probe, a variable d.c. power supply, an ammeter, and an oscilloscope. Unfortunately, the detailed interpretation of the current–voltage characteristic obtained with this setup can be quite complicated. As a result, the accuracy of the results obtained often is not as high as one would wish. Nevertheless, probe measurements have been proven very useful in characterizing plasma properties.

The plasma generated by an ion thruster is different from conventional quiescent plasmas in that the ions have a very large directed velocity. As a result, the standard interpretation of the current–voltage characteristic needs to be reconsidered.[1,2] One of the deviations from the usual situation is that the probe creates a wake that is essentially devoid of plasma. As a consequence, no current is collected at the downstream surface of the probe. A second difference is that the ion current collected by the probe will be essentially independent of the probe potential. Thirdly, the large energy of the ions striking the probe may give rise to secondary emission of electrons by the probe. This phenomenon will increase the current passing through the probe.

To guarantee that the perturbations caused by the probe to the plasma remain small, use can be made of a so-called double-probe assembly. It consists of two probes placed close together and biased electrically with respect to each other. The probe assembly is left electrically floating with respect to the plasma. Since the total current drawn from the plasma is zero, the perturbations to the plasma are limited to local effects.

Extensive previous experimentation with ion thrusters has shown that the plasma outside the thruster consists of two principal parts: the beam plasma and the charge-exchange plasma.[3–7] The beam plasma consists of ions that were accelerated by passing through the 1-kV potential difference maintained between two acceleration grids, together with neutralizing electrons. The beam plasma flows in the axial direction, spreading slightly as it travels at large distances from the thruster. The charge-exchange plasma consists of ions generated by charge-exchange collisions between energetic beam plasma ions and neutral atoms escaping through the grid. Upon generation, these ions typically will have a low energy as compared with the beam ions. Very close to the grid there is a large electric field, caused by a lack of neutralization. This field accelerates any charge-exchange ions

formed here back towards the thruster. The resulting grid erosion constitutes a serious limitation on the life of ion thrusters. Farther away from the grid, the radial component of the electric field in the beam plasma becomes important. This component accelerates the charge-exchange ions radially. These ions leave the beam region and cause the charge-exchange plasma to extend outside the main ion beam. The probability that a given neutral atom will suffer a charge-exchange collision is quite small (see Sec. VI). Because the density of neutral atoms will decrease rapidly with distance from the thruster, most of the charge-exchange collisions will take place within a few beam diameters of the outlet of the thruster. As a result, the charge-exchange plasma has its highest density near the thruster. Whereas the beam plasma is responsible for the thrust that is developed, the charge-exchange plasma is an undesirable by-product. Besides the grid erosion problem already mentioned, charge exchange ions conceivably can cause damage to spacecraft surfaces such as solar panels.

Section II describes the interpretation of results obtained with a double probe in an ion thruster plasma. The corresponding theory for a single probe is discussed in Sec. III. Section IV consists of a description of the experimental setup, while the experimental results are presented in Sec. V. The results are discussed in Sec. VI.

II. Double-Probe Theory

Consider an electric probe consisting of two parallel cylindrical electrodes perpendicular to the flow direction. An electric potential V_d is maintained between the electrodes, while the electrode assembly as a whole is kept floating electrically. The current J flowing between the electrodes can be measured as a function of the imposed voltage V_d. The following paragraphs concern the interpretation of the current-voltage characteristic obtained in this manner. In particular, it is indicated how values can be obtained for the local ion flux and electron temperature. While the treatment given is approximate, the results obtained for these two quantities should be sufficiently accurate for present purposes.

The ions in the plume of an ion thruster typically have directed energies on the order of 1000 eV. The ion temperature is much lower than that, so that the directed velocity of the ions is much larger than their average thermal speed. Provided that the plume is electrically neutral, the electron density n_{e0} in the plume equals the ion density n_{i0}. Furthermore, during steady-state operation the ion current J_i leaving the thruster must equal the electron current J_e. Together, these conditions mean that the ion current density j_i at each location in the plume must equal the electron current density j_e. Since $j_i = n_i e u_i$ and $j_e = n_e e u_e$, the directed electron velocity u_e equals the directed ion velocity u_i. For a singly charged xenon ion with an energy $E_i = m_i u_i^2/2 = 1000$ eV, this velocity is $u_i = 3.8 \times 10^4$ m/s. On the other hand, the average thermal speed of the electrons $\langle v_e \rangle = (8kT_e/\pi m_e)^{1/2} = 6.7 \times 10^5\ (kT_e$ in eV$)^{1/2}$ m/s. It can be concluded that provided kT_e is on the order of an electron volt or larger, the electrons move with a directed velocity that is much smaller than their average thermal speed.

Close to each electrode there is a thin region that is not electrically neutral. In this region, called the sheath, the potential is negative with respect to the plume plasma (see Fig. 1). Without such a negative probe-to-plasma potential, the electron flux would be equal to the thermal flux of the electrons. It is easily shown that this flux would cause the total electron current to the probe assembly to be larger than the total ion current, violating the condition that the net current to the assembly must be zero. Provided that the potential differences in the sheath are no larger than several tens of volts, the ion flux arriving at either probe equals the ion flux in the plume. In other words, the ion trajectories are essentially unaffected by the electric field in the sheath. This results

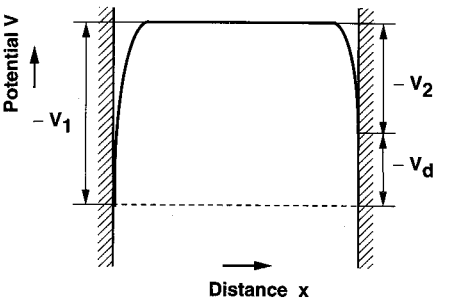

Fig. 1 Electric potential in plasma and in sheaths around probes.

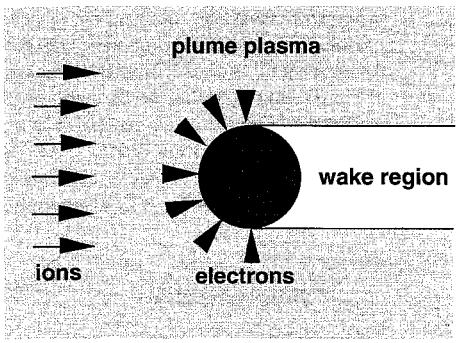

Fig. 2 Sketch of plume plasma around probe.

in a wake essentially devoid of ions behind the probe (see Fig. 2). For the conditions of interest, the major part of the wake is also essentially devoid of electrons. Near the surface dividing the wake from the plume there will be a thin sheath region containing mostly electrons. The resulting space-charge density causes the electric potential to become strongly negative, thereby preventing the electrons from entering the wake. The thickness of this sheath is on the order of the local debye length, which typically is small compared with the probe radius (cf. Appendix).

The ion current to a probe is given to a very good approximation by the product of j_i in the plume times the probe area DL projected on a plane perpendicular to the flow direction[1]:

$$J_i = n_i e u_i DL \tag{1}$$

The electron current consists of two parts: 1) electrons arriving as a result of the thermal motion of the electrons in the plume plasma and 2) electrons emitted by the probe surface as a result of the large energy of arriving ions. The latter effect is known as secondary emission resulting from ion bombardment. The average number of secondary electrons emitted per arriving ion is a strong function of the ion energy and also depends on the probe surface and the ion species. Since the probes carry a negative bias with respect to the plasma, all secondary electrons will travel toward the plasma. For given ion energy and ion species, secondary emission effectively results in amplification of the ion current by a constant factor α. If the electrons have a Maxwellian velocity distribution, their number density n_e in the sheath is given to good approximation by $n_e = n_{e0} \exp[e(V - V_{pl})/kT_e]$. The electron flux arriving at the probe then equals $j_e = j_{e0} \exp[e(V_{pr} - V_{pl})/kT_e]$, where $j_{e0} \equiv e n_{e0} \langle v_e \rangle/4 = e n_{e0}(kT_e/2\pi m_e)^{1/2}$ is the unperturbed flux. The area over which the electrons arrive equals $\pi DL/2$. Consequently, the thermal electron current arriving at the probe is given by

$$J_e = j_{e0} \exp[e(V_{pr} - V_{pl})/kT_e]\pi DL/2 \tag{2}$$

The current–voltage characteristic of the double probe follows from the condition that the net current to the probe

assembly must be zero, together with the condition that the current J flowing between the probes is the sum of the ion and electron currents to or from each probe. These conditions yield

$$2\alpha n_i e u_i DL = j_{e0}\left\{\exp\left[\frac{e(V_1 - V_{pl})}{kT_e}\right] + \exp\left[\frac{e(V_2 - V_{pl})}{kT_e}\right]\right\}\frac{\pi DL}{2} \tag{3}$$

$$2J = -j_{e0}\left\{\exp\left[\frac{e(V_1 - V_{pl})}{kT_e}\right] - \exp\left[\frac{e(V_2 - V_{pl})}{kT_e}\right]\right\}\frac{\pi DL}{2} \tag{4}$$

where the two probes are taken to have identical diameters and lengths. The result for $2J$ in Eq. (4) is obtained by taking the sum of the net current $J_{i1} - J_{e1}$ arriving at probe 1 and the net current $-J_{i2} + J_{e2}$ leaving probe 2. Eliminating j_{e0}, setting $V_1 - V_2$ equal to V_d (i.e., neglecting the potential drop in the plasma outside the sheaths) and solving for the dimensionless current $\bar{J}$ results in

$$\bar{J} \equiv \frac{J}{\alpha n_i e u_i DL} = \frac{\exp(eV_d/kT_e) - 1}{\exp(eV_d/kT_e) + 1} = \tanh(\phi_d/2) \tag{5}$$

where $\phi_d = eV_d/kT_e$. Limiting cases are

$$\bar{J} \cong 1 \quad \text{for} \quad \phi_d >> 1 \tag{5a}$$

$$\bar{J} \cong -1 \quad \text{for} \quad \phi_d << -1 \tag{5b}$$

For small values of ϕ_d, a Taylor series expansion of Eq. (5) yields

$$\bar{J} \cong \phi_d/2 - \phi_d^3/24 \quad \text{for} \quad |\phi_d| << 1 \tag{5c}$$

Cases (5a) and (5b) are said to represent saturation. The current in these cases is limited by the ion current arriving at one of the probes. Apart from the factor α, these are the standard results for double electric probes.[8] Denoting the current $\alpha e n_i u_i DL$ collected at saturation by J_{sat}, it follows that the ion flux $n_i u_i$ can be determined from

$$n_i u_i = \frac{J_{sat}}{\alpha eDL} \tag{6}$$

Differentiating Eq. (5c) with respect to J and setting V_d equal to zero yields the electron temperature

$$\frac{kT_e}{e} = \frac{1}{2} J_{sat}\left(\frac{dV_d}{dJ} \quad \text{at} \quad V_d = 0\right) \tag{7}$$

The coefficient α must follow either from known data about secondary emission or from measurements throughout the plume together with the known total ion current. For the case of xenon atoms striking a tungsten surface at an energy of 1000 V, α is reported to be 1.019 (Ref. 9, Table 9.2, p. 777). Since this differs from unity by less than 2%, the influence of secondary emission is negligible under these conditions.

An additional quantity of interest is the floating potential $V_f - V_{pl}$, which is the potential that an electrically floating probe will have with respect to the plasma potential V_{pl}. The value of $V_f - V_{pl}$ follows from equating the ion and electron currents collected by the probe. Under present conditions the result depends on the geometry of the probe. For a cylindrical probe oriented perpendicular to the flow direction, the result is

$$\alpha e n_i u_i DL = e n_{e0}(\langle \text{lt} v_e \rangle/4)\exp[e(V_f - V_{pl})/kT_e]\pi DL/2$$

$$\text{or} \quad \frac{e(V_f - V_{pl})}{kT_e} = \ln \alpha + \frac{1}{2}\ln\left(\frac{16E_i m_e}{\pi kT_e m_i}\right) \tag{8}$$

The latter expression equals $-1.93 - 0.5 \ln(kT_e$ in eV) for xenon ions at $E_i = 1000$ eV and $\alpha = 1$. Here it is assumed that $V_f - V_{pl} < 0$, i.e., that $kT_e > 0.021$ eV. For positive values of $V_f - V_{pl}$, the assumption that the electron current is proportional to the Boltzmann factor $\exp[e(V_f - V_{pl})/kT_e]$ is invalid.

The validity of the assumption that both probes are biased negatively with respect to the plasma even at saturation can be tested as follows. Consider the limiting case that the electron-attracting probe in the saturation regime is at the same potential as the plasma. Equating the total ion current to the electron current yields for probes of equal dimensions

$$2\alpha e n_i u_i DL = e n_{e0}(\langle v_e \rangle/4)\pi DL/2 \quad \text{or} \quad kT_e = \frac{64\alpha^2 E_i m_e}{\pi m_i} \tag{9}$$

The latter expression equals 0.085 eV for xenon ions at 1000 eV and $\alpha = 1$. For values of kT_e larger than this threshold, the assumption is justified. Note that the present threshold differs by a factor of 4 from the value 0.021 eV corresponding to $V_f - V_{pl} < 0$. The difference arises because in the present case, the electron current balances the ion current to both probes rather than to just one, and because the electron thermal flux is proportional to $T_e^{1/2}$.

Under the assumptions stated, the results obtained are independent of the thickness of the sheaths around the probes. They also are independent of other complications that arise in conventional langmuir probes, such as the effects of orbital motion and of the sheath criterion applicable when the electron temperature is greater than the ion temperature. Nevertheless, it is of interest to determine the thickness of the sheaths surrounding the present probes. Under the experimental conditions of present interest, the thickness of the sheath typically is small compared with the probe radius at values of the probe potential close to the plasma potential, and on the order of the probe radius when the probe potential is about 5 V below the plasma potential (see Appendix).

III. Single-Probe Theory

The most common application of electric probes is to record the current–voltage characteristic of a single probe in the form of a thin wire. The underlying assumption is that the plasma is at a fixed electric potential, so that varying the potential of the probe will be equivalent to varying the potential drop between the probe and the plasma. In practice, this means that the plasma potential is maintained by some other electrical conductor, e.g., the anode in an electrical discharge. There typically is a potential difference between the other electrical conductor and the plasma. As a result, the current–voltage characteristic of a single probe does not pass through the origin as it does for a double probe. Instead, the probe voltage at zero current represents the floating potential V_f of the probe with respect to the plasma (Fig. 3). The absolute value of the probe potential at this point depends on how the probe is biased with respect to the electrical conductor maintaining the plasma potential.

Provided that the electrons in the beam plasma have a nearly Maxwellian velocity distribution and the electron flux attracted by the probe is small compared with the electron

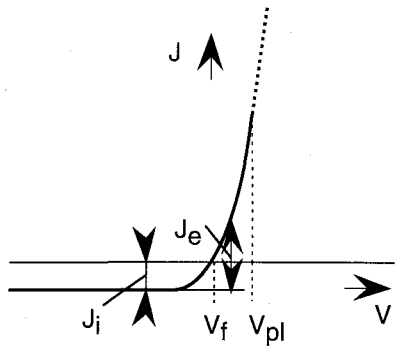

Fig. 3 Current–voltage characteristic of a single probe.

thermal flux, the current–voltage characteristic of a single cylindrical probe in an ion thruster plasma is given by

$$J = -\alpha e n_i u_i DL + e n_{e0} \frac{\langle v_e \rangle}{4} \exp\left[\frac{e(V - V_{pl})}{kT_e}\right] \frac{\pi DL}{2} \tag{10}$$

This result is applicable when the probe potential is sufficiently small ($V \approx V_f$ or less in Fig. 3). Using the condition $V = V_f$ at $J = 0$, it can be recast in the form

$$\frac{J}{J_{sat}} + 1 = \exp\left[\frac{e(V - V_f)}{kT_e}\right] \tag{11}$$

The electron temperature can be determined by plotting

$$\ln[(J/J_{sat}) + 1] \quad \text{vs} \quad V - V_f \tag{12}$$

Provided that the electrons indeed have a Maxwellian velocity distribution, this plot yields a straight line in the region of small V, and the inverse slope of this line equals kT_e/e. Any deviations from a straight line provide information about the actual velocity distribution function. The possibility of obtaining information about this function over the entire range of V constitutes a principal advantage of a single probe over a double probe. The other principal advantage is the determination of the floating potential, which provides information about the neutralization process.

IV. Description of Experiment

The experimental work was carried out in the ion beam of a UK-10 ion thruster.[10,11] The thruster was run at conditions providing a nominal thrust of 18 mN: beam current 0.33 A, beam voltage 1100 V, anode current 2 A, cathode keeper current 1 A, neutralizer keeper current 0.66 A, magnet current 160 mA, accelerator grid current 1.5 mA, accelerator grid voltage −340 V, main xenon flow rate 0.62 mg/s, cathode xenon flow rate 0.110 mg/s, and neutralizer xenon flow rate 0.036 mg/s. The experiments were carried out in a vacuum chamber having a diameter of 2.4 m and a length of 5.5 m. The ion beam ended up at a grounded beam dump about 2.2 m from the thruster. The vacuum in the chamber was maintained by two CVI Torrmaster TM1200 cryopumps, supported by a Leyboldt TMP/NT 150/360V/H turbomolecular pump. During the experiments most of the background gas was xenon at a pressure of about 2×10^{-6} torr (0.3 mPa). This pressure was measured with an ionization gauge, using the xenon/air correction factor of 0.33. The electric probe was mounted on a Compumotor Model 4000 Positioning System, which allowed horizontal motion along the beam direction from 5 to 60 cm from the thruster grid. Most measurements were carried out in the horizontal plane containing the beam axis; the range of motion perpendicular to the beam axis in this plane was 28 cm. The range of vertical motion was slightly

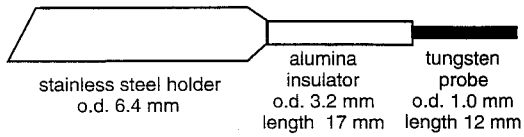

Fig. 4 Sketch of single-probe configuration.

larger than that. During the experiments, the center of the neutralizer was located 6.2 cm below the beam center. Its horizontal distance from the center was −5.7 cm, using the sign convention adopted in the figures shown in the next section. The configuration of the single probe is sketched in Fig. 4. The double probe consisted of two such configurations with slightly different dimensions (probe length 13 mm instead of 12 mm, alumina length 25 mm instead of 17 mm, alumina o.d. 4.5 mm instead of 3.2 mm). A spacer was mounted between the two steel holders, which kept the two tungsten wires 9 mm apart vertically. Keeping the probes separate prevented shorting between them by sputtering deposits. The wires were perpendicular to the axis of the ion beam during the measurements. Voltage on the single probe was varied from 0 to 15 V with respect to ground, with increments of 0.25 V. The double-probe assembly was made to float electrically. The voltage difference supplied to the assembly was varied from −5 to +5 V with increments of 0.1 V for most of the measurements, and from −15 to +15 V with increments of 0.5 V for some additional measurements in the central part of the beam. These voltages were provided by a Kepco model BOP100-1M bipolar operational power supply/amplifier. The current supplied to the probes was measured as the voltage drop across a 1.00 kΩ resistance in series with the probe. This voltage drop was recorded using a Fluke model 8840A multimeter. A second Fluke 8840A provided an accurate record of the voltage across the probes. All measurements were taken with a computerized data acquisition system. The data obtained were stored in ASCII files and were evaluated by computer analysis.

V. Experimental Results

Representative current–voltage characteristics obtained with the single probe and the double probe are shown in Figs. 5a and 5b, respectively. The traces shown consist of straight-line segments between adjacent experimental data points. As indicated on the figure, the solid curve is plotted using the axis on the right-hand side (RHS) while the other two curves are plotted using the axis on the left-hand side (LHS).

Horizontal profiles of the ion flux $n_i u_i$ are shown in Figs. 6a (single-probe results) and 6b (double-probe results). The traces consist of straight-line segments between experimental data points that were taken 0.64 cm apart. The ion flux is seen to have a maximum at about 15 ± 0.3 cm from the grid. This maximum is the result of the inward curvature of the UK-10 accelerator grid system, resulting in a waist of the ion beam. The waist was clearly noticeable in the blue glow by which the ion beam manifested itself visually. The results shown in Figs. 6a and 6b are seen to be in very good agreement with each other. They also are in good qualitative agreement with the preliminary data obtained with a Faraday-cup ion probe by Harvey et al.[12] Assuming that the ions all strike the probe perpendicularly with a kinetic energy of 1100 eV, the ion profiles also represent ion density profiles. The corresponding ion density scale is shown on the right of Fig. 6. The maximum ion density at the beam waist is $1.8 \pm 0.2 \times 10^{10}$ cm^{-3}. Figure 7 shows a vertical ion flux profile taken at a distance of 60 cm from the grid, together with the horizontal ion flux profile at that location. The line representing the latter again consists of straight-line segments between experimental data points. The good agreement between the two profiles is consistent with the beam being axisymmetric to a good approximation. Making use of this axisymmetry allows

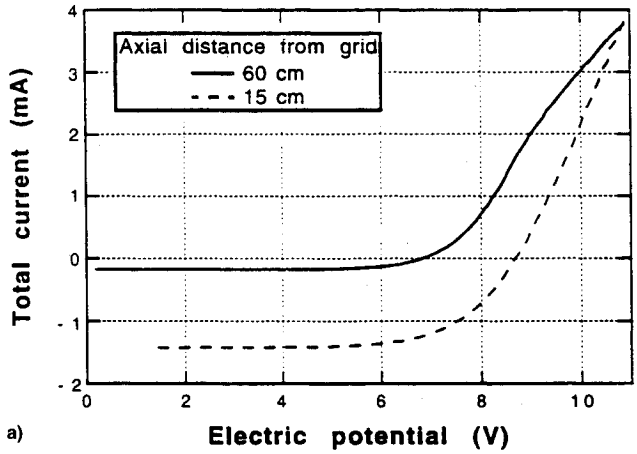

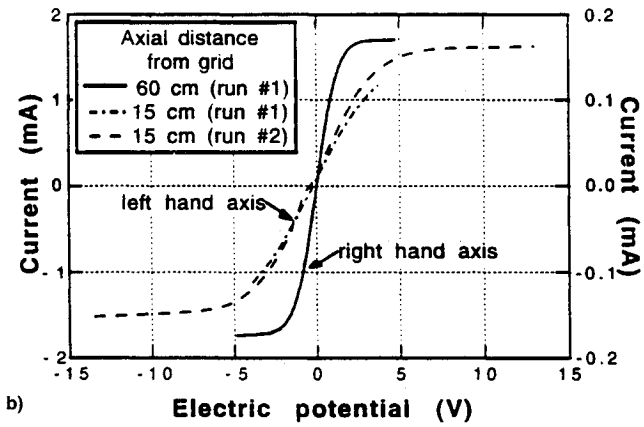

Fig. 5 Representative current–voltage characteristics: a) single and b) double probe.

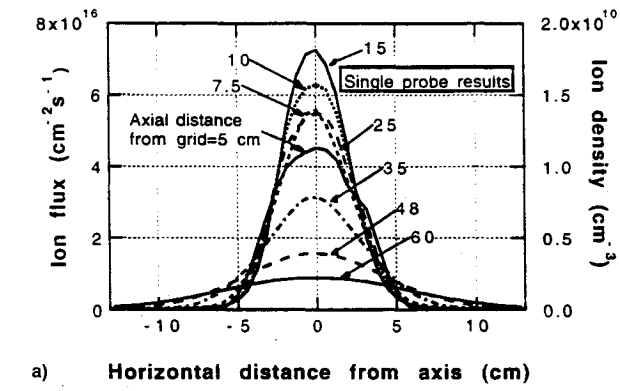

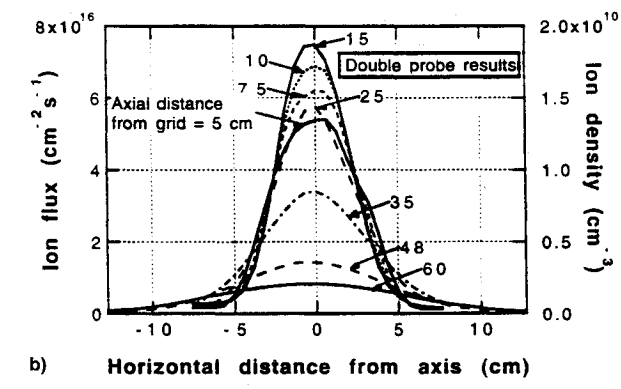

Fig. 6 Horizontal profiles of ion flux: a) single- and b) double-probe results.

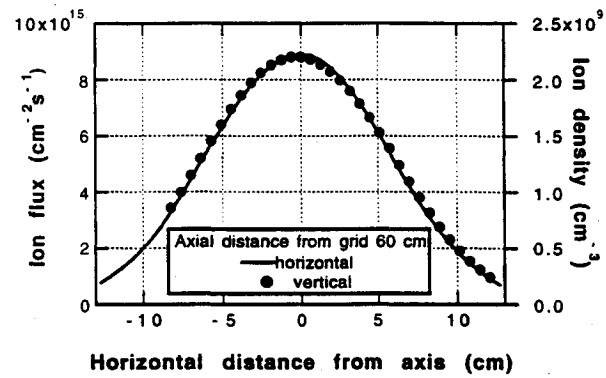

Fig. 7 Vertical and horizontal ion flux profiles.

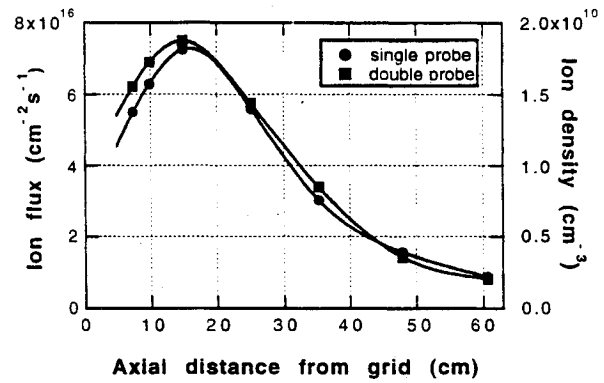

Fig. 8 Axial ion flux profile along centerline.

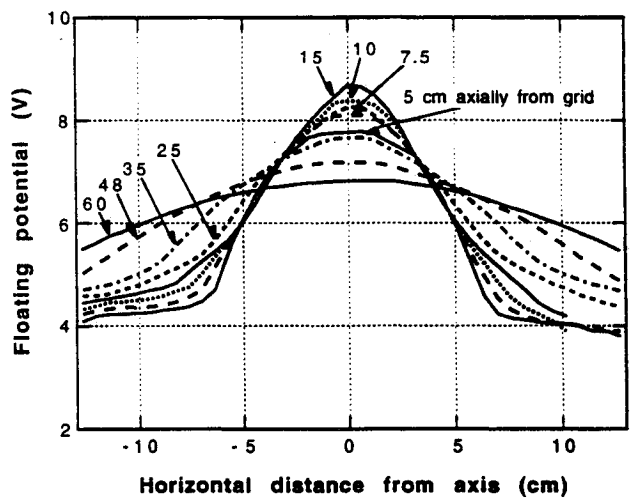

Fig. 9 Horizontal profiles of floating potential.

determination of the total beam current by integrating the ion flux profiles. The result was found to be about 0.30 ± 0.03 A at axial distances of both 5 and 60 cm from the grid. This indicates that ion–electron recombination and charge exchange collisions between 5–60 cm have negligible effect on beam current within experimental accuracy. The integrated beam current result of 0.30 ± 0.03 A is quite close to the measured beam current of 0.33 ± 0.01 A. Axial profiles of ion flux are shown in Fig. 8. The points represent the experimental data, the lines are cubic spline fits through the data. The figure again shows the existence of the ion beam waist at about 15 cm from the grid.

Figure 9 shows horizontal profiles of the electric floating potential V_f, determined by the value of the potential at which no current is collected by the single probe. The traces again consist of straight line segments between experimental data

points. The values shown are the potential with respect to ground. Since the outside of the neutralizer was at ground potential, the values shown are indicative of the electric potential to which the electrons are subjected upon leaving the neutralizer. There clearly is a large potential well for electrons in the center of the beam. As can be seen in Fig. 10, this well is deepest at the waist of the beam. The floating potential at that location is 8.5 ± 0.2 V with respect to the neutralizer. The line in Fig. 10 again is a cubic spline fit through the data points.

Results for the floating potential in three planes perpendicular to the beam axis near the thruster outlet are given in Fig. 11. The profiles generally are symmetric about the centerline. There are no large differences between the profiles of the three planes.

In principle, single-probe data can provide information on characteristic electron energies. To this purpose, the electron current is obtained by subtracting the ion saturation current from the total current, with the saturation current defined as the total current at the smallest voltage. The logarithm of the electron current then is plotted as a function of potential. The results for the traces of Fig. 5a are shown in Fig. 12. If the electron velocity distribution is Maxwellian, such a plot should yield a straight line at small values of the current. The electron temperature in this case equals the inverse slope of the line. The straight line should extend over the range where the electron flux remains small compared with the mean electron thermal flux. Inspection of Fig. 12 shows that such a straight line is not obtained, indicating that the electron velocity distribution is non-Maxwellian. To illustrate this further, an approximate plot of the distribution function was obtained using the procedure described in Ref. 8, Sec. 3.2.2. This procedure is based on the assumption that the distribution function is isotropic, and that the sheath is thin compared with the radius of the probe. In this case, the distribution function of electron speed (=magnitude of velocity) is obtained by double differentiation of the J-V characteristic, followed by multiplication with the potential difference between probe and plasma. The double differentiation yields a curve that is positive at small values of V, but becomes negative at large V. In carrying out this procedure, the plasma potential was taken as the value of V for which the curve passes through the V axis. Also, the original J-V curve was smoothed twice, using the binomial smoothing filter described by Marchand and Marmet,[13] as implemented in the IGOR Graphing and Data Analysis computer program. The results for the data at 15 cm from the grid are shown in Fig. 13, together with the original J-V characteristic. Also shown is a Maxwellian fit to the speed distribution. This fit was obtained using the equation $g = C_1(V_{pl} - V)\exp[-C_2(V_{pl} - V)]$ with $C_1 = eg_m/(V_{pl} - V_m)$ and $C_2 = 1/(V_{pl} - V_m)$, where subscript m denotes the maximum of

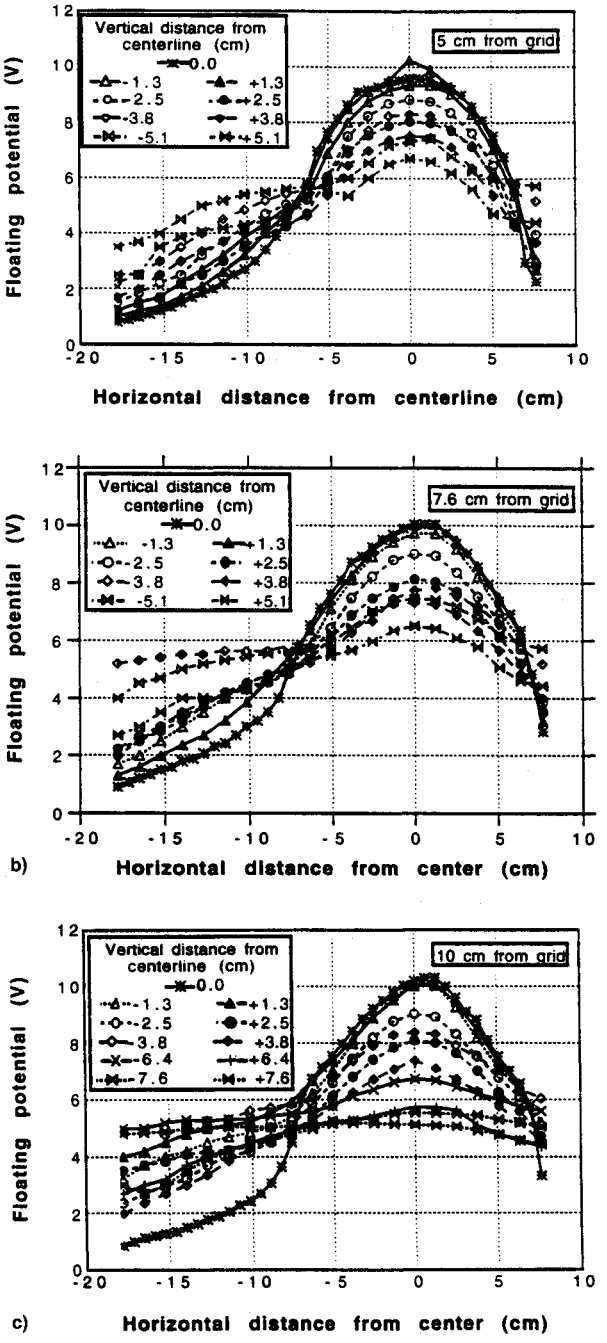

Fig. 11 Floating potential profiles in planes perpendicular to beam axis. Distance from grid: a) 5, b) 7.6, and c) 10 cm.

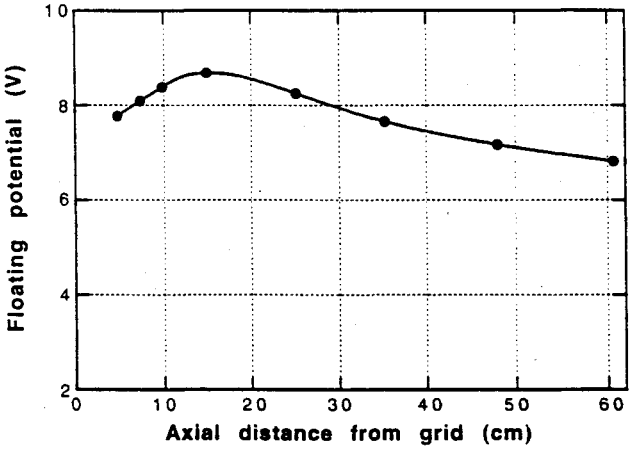

Fig. 10 Floating potential along centerline.

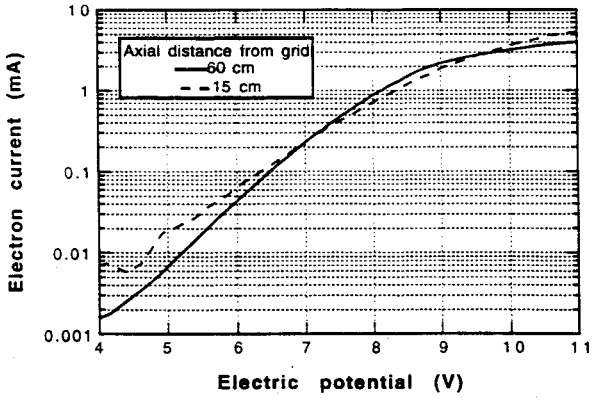

Fig. 12 Semilogarithmic plot of electron current.

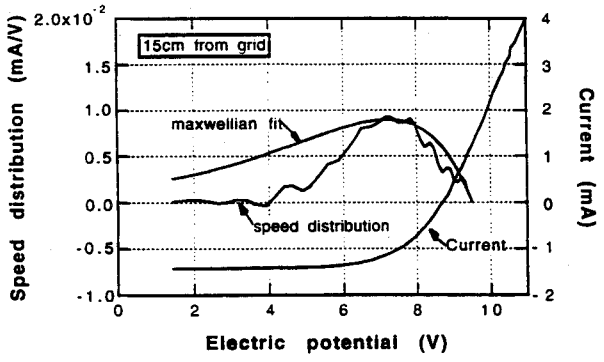

Fig. 13 Electron speed distribution derived from the curve at 15 cm from the grid shown in Fig. 5a, reproduced here with the label Current.

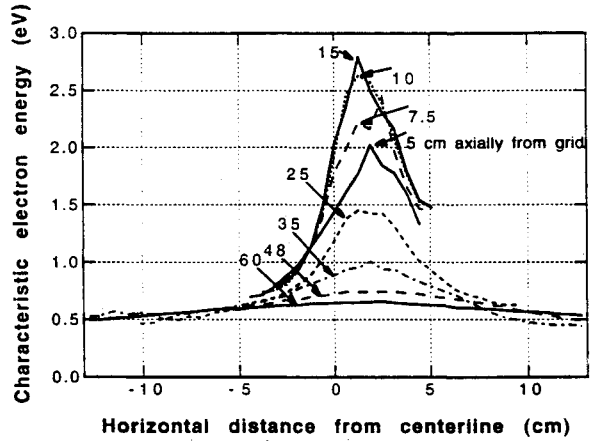

Fig. 14 Characteristic electron energy (double probe).

the experimentally derived distribution function. The result indicates that the tail of the actual speed distribution function is relatively empty compared with the main part of the function. Similar results can be obtained at other locations. A possible explanation of the relative emptiness of the tail is discussed in Sec. VI. For completeness, it should be noted that the procedure followed in determining the speed distribution function is not always successful. As a consequence, results such as represented by Fig. 13 should be considered tentative.

If the electron distribution function is not Maxwellian, the electron temperature is no longer defined as usual. The *J-V* characteristics obtained with the double and the single probe were still evaluated using the procedures that usually yield electron temperature. The results are shown as characteristic electron energies in Figs. 14 and 15, respectively. The double probe results of Fig. 14 were obtained using the procedure described in Sec. II. The data shown at 60, 48, 35, and 25 cm from the grid are based on *J-V* traces in which the voltage was varied from −5 to +5 V by 0.1-V increments (referred to as run #1 in Fig. 5b). The remaining data are based on traces in which the voltage was varied from −15 to +15 V by 0.5-V increments (run #2 in Fig. 5b). The slope at the origin was determined by applying the method of least-mean-squares to the five points closest to the origin. It is seen that the characteristic electron energy has a maximum of about 2.7 ± 0.3 eV near the waist, and gradually decreases to about 0.6 ± 0.1 eV between the waist and an axial distance of 60 cm. The results indicate that the maximum of the characteristic electron energy occurs at 1–2 cm beyond the centerline, on the side opposite to the neutralizer. The single-probe results shown in Fig. 15 are based on the traces of Fig. 5a. At each position in space the inverse slope was evaluated for the five points in the range $V_f \rightarrow V_f + 1.25$ V. This slope again

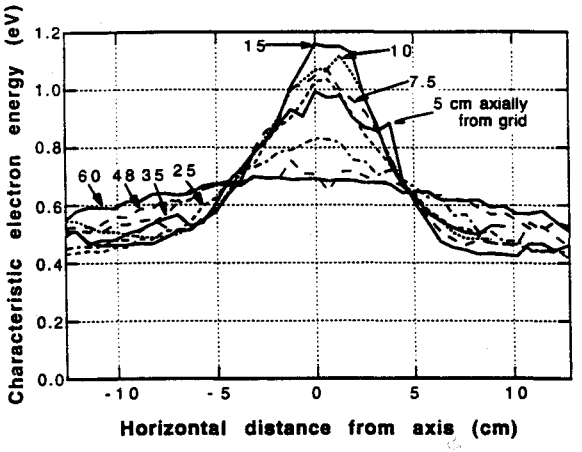

Fig. 15 Characteristic electron energy (single probe).

was found using the method of least-mean-squares. Near the waist of the ion beam this procedure yields values of electron temperature that are considerably lower than the corresponding characteristic electron energies shown in Fig. 14. The maximum value in this case is 1.2 ± 0.1 eV. This discrepancy is unexpected, since both the single- and double-probe results are based on the part of the *J-V* characteristic close to the floating potential. As a consequence, both results represent the region of the electron velocity distribution corresponding to the potential difference between plasma and floating potential. It may be that the discrepancy is caused by variations in the potential of the beam plasma in the case of a single probe. Such variations were assumed absent in the determination of characteristic electron energies from single-probe data (see Sec. III, second sentence). All of the energies represented in Figs. 14 and 15 are larger than the characteristic energies corresponding to the linear part of the corresponding $/\!/ J_e$ vs V plots. The latter energies represent the high energy tail of the distribution function, and are on the order of 0.5–0.8 eV.

The extent to which the plasma is neutralized can be estimated using Poisson's equation

$$\nabla^2 V_{pl} = -e[(n_i - n_e)/\varepsilon_0] \tag{13}$$

where $\varepsilon_0 = (1/36\pi) \times 10^{-9}$ A s/(V m). With V_f known from Fig. 9 and $V_f - V_{pl}$ estimated from Eq. (8), numerical values can in principle be obtained for the LHS of Eq. (13). A lower estimate of $n_i - n_e$ is obtained by neglecting the contribution from $V_f - V_{pl}$, i.e., by using the results of Fig. 9 for V_f instead of V_{pl} in Eq. (13). At the center of the beam waist this yields $n_i - n_e \approx 3 \times 10^5$ cm^{-3}. An upper estimate is obtained by including the contribution from $V_f - V_{pl}$ determined by using Eq. (8) together with Fig. 14 for T_e. This yields $n_i - n_e \approx 2 \times 10^6$ cm^{-3}. However, as discussed previously, Fig. 14 does not actually represent T_e, so that the value just quoted is only an order of magnitude estimate. This value constitutes a fraction of $\approx 10^{-4}$ of the local ion density. The fraction $(n_i - n_e)/n_e$ can be called the degree of nonneutralization. A similar order of magnitude estimate yields $n_i - n_e \approx 3 \pm 1 \times 10^4$ cm^{-3} at the beam axis 60 cm from the grid, with approximately equal contributions coming from Fig. 9 and from Eq. (8) together with Fig. 14. The latter value is equivalent to a degree of nonneutralization of $\approx 10^{-5}$.

VI. Discussion

One of the interesting questions arising in connection with ion thrusters concerns the neutralization mechanism. The effective mean free path (mfp) l for momentum transfer of an electron in the ion beam can be estimated by using the relation $l \approx 1/(n_i \sigma_{ei})$, where σ_{ei} is the effective electron–ion collision

section for the transfer of momentum. An order of magnitude estimate for this cross section is $\sigma_{ei} \approx 6.5 \times 10^{-13}/\varepsilon^2$ cm^2, where ε is the electron energy in eV.[14] Taking $\varepsilon = 8$ eV (representative of the potential difference between the outside of the neutralizer and the centerline of the ion beam) and $n_i = 1.5 \times 10^{10}$ cm^{-3} yields $l \approx 70$ m. This is also the effective mfp for electron–electron momentum and energy transfer (the effective mfp for electron–ion energy transfer is larger by the ion–electron mass ratio). Upon being pulled into the beam by the electric potential difference between neutralizer and beam, an electron will tend to pass right through the beam. It will then emerge on the other side having the same energy with which it entered. Newly entered electrons thus will oscillate back and forth through the beam. During this oscillation process, electrons will transfer energy and momentum to each other. There is no guarantee that the velocity distribution of the resulting electron gas is Maxwellian. In fact, two circumstances make it likely that the distribution function is non-Maxwellian. These are that the effective mfp is large compared with the characteristic macroscopic distances such as the beam diameter and that the effective mfp increases with electron energy. Because of the latter circumstance, high-energy electrons can escape in the axial direction. This mechanism might explain the relative emptiness of the speed distribution function shown in Fig. 13.

Another way in which electrons that have newly entered the ion beam might be influenced is by means of plasma oscillations. Such oscillations have been reported by Bernstein and Sellen,[15] who suggested that they are caused by a two-stream instability between the entering electron stream and the electrons in the beam plasma.

The present results are principally concerned with the beam plasma. As was pointed out by Carruth,[7] accurate property values of the charge-exchange plasma are much harder to obtain. The ions in the latter plasma do not have a very large energy, nor is their energy uniform. Also, they do not all travel in essentially the same direction. The charge-exchange plasma has its origin in neutral atoms that escape through the acceleration grids. The charge-exchange cross section for Xe^- ions and Xe atoms in the kilovolt range has been measured to be about 5×10^{-15} cm^2 (Ref. 16). In an ion flux of 6×10^{16} cm^{-2}s^{-1}, it follows that the mean time between exchange collisions of an atom is about 3.3×10^{-3} s. During this time, a xenon atom moves over a distance 4.0 (kT in eV)$^{1/2}$ m, where kT is the kinetic energy of the atom. For any reasonable value of kT, this distance is large compared with the beam diameter. It can be inferred that most of the neutrals do not suffer charge-exchange collisions, and leave the thruster in the form of a free expansion into the vacuum. Their density will be highest close to the thruster. As a consequence, the density of the charge-exchange plasma will also be highest close to the thruster.

While the interpretation of the J-V characteristic in the charge-exchange plasma is quite complicated, there still exist reported values of ion energy and electron density in this region.[7] Typical values of the electron density here are on the order of 10^7–10^8 cm^{-3}. Present results for the ion flux collected outside the beam plasma are shown in Fig. 16, which is identical to Fig. 6a except that a logarithmic scale is used for the vertical axis. The conversion of ion flux to ion density used in Fig. 6a is not applicable in the charge-exchange plasma. It would lead to values of the ion density that are lower than the actual values, because the energy of the ions in the charge-exchange plasma is much smaller than 1100 eV. In addition, various geometrical effects influence the conversion factor. Nevertheless, a crude estimate indicates that n_i values in the present case may also be on the order of 10^7–10^8 cm^{-3}. An example of the J-V characteristic obtained with the single probe outside the beam is shown in Fig. 17. Another crude estimate indicates that the electron density may be of the order of 10^8 cm^{-3} at the location where this characteristic was

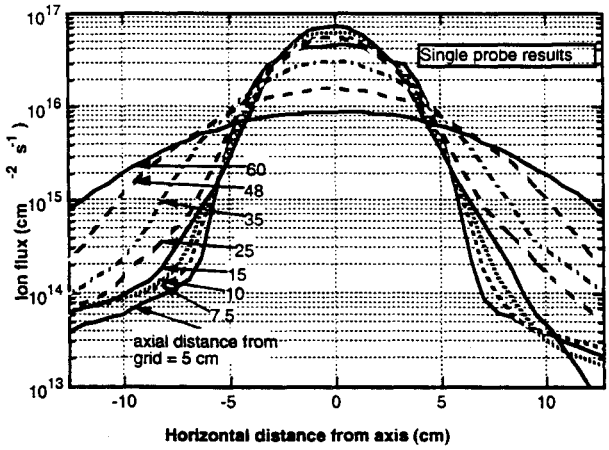

Fig. 16 Single-probe result for horizontal profiles of ion flux (same as Fig. 6a, except that the vertical scale here is logarithmic).

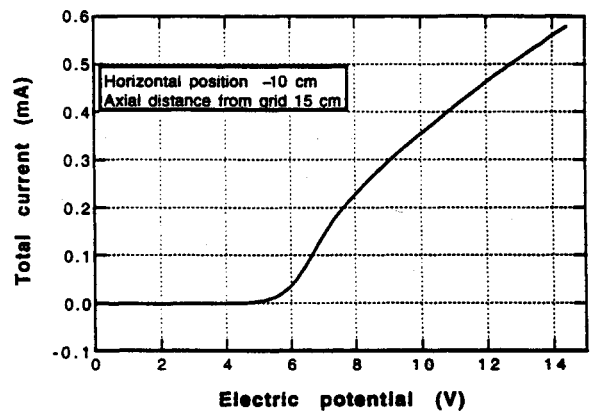

Fig. 17 Typical current–voltage characteristic obtained with single probe outside the ion beam.

obtained. Further work is needed for an accurate determination of the properties of the charge-exchange plasma.

In conclusion, it may be stated that electric probes of the kind described are useful tools in determining properties of the beams produced by ion thrusters. The probes are especially useful in measuring ion flux profiles in the beam plasma as well as floating potential profiles and degree of nonneutralization. The probes also provide information about the characteristic energy of the electrons. Results of this type are of interest to spacecraft designers and can be used to verify the validity of computer models for the properties of ion beams (see, e.g., Ref. 17).

Appendix: Estimate of Sheath Thickness

As mentioned at the end of Sec. II, it is of interest to estimate the thickness of the sheath surrounding the probe. In the following lines this estimate is made assuming cylindrical symmetry, i.e., neglecting the existence of the ion wake and the finite length of the probe. The Poisson equation for the cylindrically symmetric case is

$$\frac{1}{r}\frac{\mathrm{d}}{\mathrm{d}r}\left[r\frac{\mathrm{d}(-V)}{\mathrm{d}r}\right] = \frac{e}{\varepsilon_0}(n_i - n_e) \qquad \text{(A1)}$$

The solution is subject to the boundary conditions $V = V_{pr}$ at $r = r_p$, $V = V_{pl}$ and $\mathrm{d}V/\mathrm{d}x = 0$ at $r = \infty$. The ion density n_i is assumed equal to the freestream value n_{e0} of the electron density, while the electron density n_e is assumed to be given by

$$n_e = n_{e0}\exp[e(V - V_{pl})/kT_e] \qquad \text{(A2)}$$

Nondimensionalizing by setting

$$\eta \equiv -\frac{e(V - V_{pl})}{kT_e} (>0), \quad \rho \equiv r/\lambda_D, \quad \lambda_D^2 \equiv \frac{\varepsilon_0 kT_e}{n_{e0}e^2} \tag{A3}$$

results in

$$\frac{1}{\rho}\frac{d}{dr}\left(\rho\frac{d\eta}{d\rho}\right) = 1 - e^{-\eta} \tag{A4}$$

For small $\eta_{pr} \equiv -e(V_{pr} - V_{pl})/kT_e$, the RHS can be approximated by η. The resulting equation can be solved by setting

$$\eta = \rho^{-1/2}e^{-\rho}g(\rho) \tag{A5}$$

where $g(\rho)$ is subject to the equation

$$g - 2\eta^2 g' + \eta^2 g'' = 0 \tag{A6}$$

This equation can be satisfied by the power series

$$g(\rho) = \sum_{n=0}^{\infty} a_n \rho^{-n} \tag{A7}$$

with the recursion relation

$$a_{n+1} = -a_n(4n^2 + 4n + 1)/[8(n + 1)] \tag{A8}$$

Equation (A5) satisfies the boundary conditions at $\rho = \infty$. Using the boundary condition $\eta = \eta_{pr}$ at $\rho = \rho_{pr}$ yields the final solution in the form of the asymptotic series:

$$\frac{\eta}{\eta_{pr}} = \left(\frac{\rho}{\rho_{pr}}\right)^{1/2} \exp[-(\rho - \rho_{pr})] \times \frac{1 - (1/8\rho) + (7/256\rho^2) - \cdots}{1 - (1/8\rho_{pr}) + (7/256\rho_{pr}^2) - \cdots} \tag{A9}$$

The factor $\exp[-(\rho - \rho_{pr})]$ indicates that the effective sheath thickness is on the order of a debye length λ_D. Numerically, this length is found from

$$\lambda_D = 7430\sqrt{(kT_e \text{ in eV}/n_e \text{ in cm}^{-3})} \text{ mm} \tag{A10}$$

Taking $kT_e \cong 1$ eV and $n_{i0} = 1.8 \times 10^{10}$ cm^{-3}, it is found that λ_D is on the order of 0.05 mm on the centerline at 15 cm from the grid. Taking the same value for kT_e and $n_{i0} = 0.2 \times 10^{10}$ cm^{-3}, it follows that λ_D is on the order of 0.2 mm at 60 cm from the grid.

For large η_{pr} the value of $e^{-\eta}$ is much less than 1 over most of the sheath, so that the RHS of Eq. (A4) can be approximated by 1. The solution of Eq. (A4) satisfying the boundary condition at $\rho = \rho_{pr}$ then is

$$\eta = \eta_{pr} + \tfrac{1}{2}(\rho^2 - \rho_{pr}^2) - \tfrac{1}{2}\rho_s^2 \ln\frac{\rho}{\rho_{pr}} \tag{A11}$$

Using the boundary condition $\rho = \rho_s$ at $\eta = 0$, it follows that

$$\frac{\eta_{pr}}{\rho_{pr}^2} = \frac{1}{4}\left(\frac{\rho_s^2}{\rho_{pr}^2} - 1\right) + \frac{1}{2}\frac{\rho_s^2}{\rho_{pr}^2}\ln\frac{\rho_s}{\rho_{pr}} \tag{A12}$$

which provides ρ_s/ρ_{pr} as a function of η_{pr}/ρ_{pr}^2. This function is plotted in Fig. A1. The value of η_{pr}/ρ_{pr}^2 follows from

$$\frac{\eta_{pr}}{\rho_{pr}^2} = -\frac{\varepsilon_0(V_{pr} - V_{pl})}{en_{i0}r_{pr}^2} = 2.21 \times 10^8 \frac{(-V_{pr} + V_{pl} \text{ in V})}{n_{i0} \text{ in cm}^{-3}} \tag{A13}$$

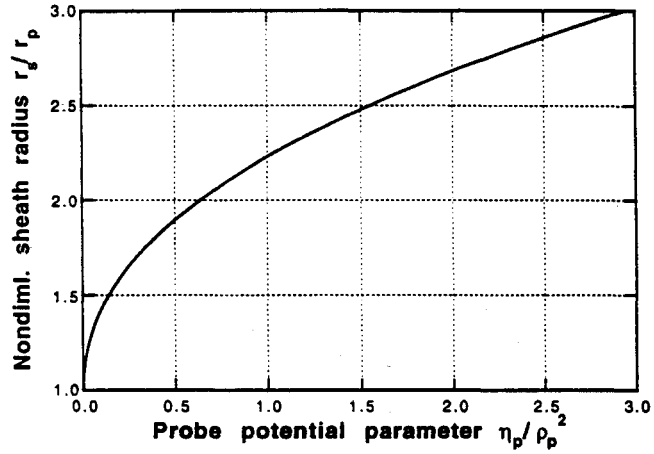

Fig. A1 Nondimensional sheath radius as function of probe potential parameter η_{pr}/ρ_{pr}^2, for case of large probe potential η_{pr}.

Taking $-(V_{pr} - V_{pl}) = 5$ V and $n_{i0} = 1.8 \times 10^{10}$ cm^{-3}, it is found that on the centerline at 15 cm from the grid $\eta_{pr}/\rho_{pr}^2 = 0.061$ and $r_s/r_p = 1.33$, so that the sheath thickness $r_s - r_p \cong 0.16$ mm. Similarly, with $-(V_{pr} - V_{pl}) = 5$ V and $n_{i0} = 0.2 \times 10^{10}$ cm^{-3}, it is found that on the centerline at 60 cm from the grid $\eta_{pr}/\rho_{pr}^2 = 0.55$ and $r_s/r_p = 1.9$, so that $r_s - r_p \cong 0.47$ mm.

Acknowledgments

This work was sponsored by the U.S. Air Force's Space and Missile Systems Center, Division of Advanced Plans under Contract FO4701-88-C-0089, with funds provided by the Foreign Comparative Test Program of the Secretary of the Air Force. The experimental setup was designed by R. B. Cohen, M. W. Crofton, S. W. Janson, L. K. Johnson, and J. E. Pollard. D. G. Fearn of the U.K.'s Defense Research Agency (Farnborough) provided the UK-10 thruster. N. Wallace of the Defense Research Agency was of crucial assistance during initial operation of the thruster. The major part of the data acquisition program was written by H. Baumgartner. E. W. Fournier provided invaluable help in finalizing this program, as well as in writing the data analysis programs.

References

[1]Segall, S. B., and Koopman, D. W., "Application of Cylindrical Langmuir Probes to Streaming Plasma Diagnostics," *Physics of Fluids*, Vol. 16, No. 7, 1973, pp. 1149–1156.

[2]Clayden, W. A., *Rarefied Gas Dynamics*, edited by J. Laurman, Vol. II, Academic, New York, 1963, p. 435.

[3]Kaufman, H. R., "Charge-Exchange Plasma Generated by an Ion Thruster," NASA CR-134844, Dec. 1975, and CR-135318, Dec. 1977.

[4]Byers, D. C., "Electron Bombardment Thruster Field and Particle Interfaces," *Journal of Spacecraft and Rockets*, Vol. 16, No. 5, 1979, pp. 289–301.

[5]Carruth, M. R., Jr., and Brady, M. E., "Measurement of the Charge-Exchange Plasma Flow from an Ion Thruster," *Journal of Spacecraft and Rockets*, Vol. 18, No. 5, 1981, pp. 457–461.

[6]Carruth, M. R., Jr., Gabriel, S. B., and Kitamura, S., "Ion Thruster Charge-Exchange Plasma Flow," *Journal of Spacecraft and Rockets*, Vol. 19, No. 6, 1982, pp. 571–578.

[7]Carruth, M. R., Jr., "A Review of Studies on Ion Thruster Beam and Charge-Exchange Plasmas," AIAA Paper 82-1944, Nov. 1982.

[8]Chen, F. F., "Electric Probes," *Plasma Diagnostic Techniques*, edited by R. H. Huddlestone and S. L. Leonard, Academic, New York, 1965.

[9]Loeb, L. B., *Basic Processes of Gaseous Electronics*, Univ. of California Press, Berkeley, CA, 1960.

[10]Fearn, D. G., Martin, A. R., and Smith, P., "Ion Propulsion Research and Development in the UK," *Journal of the British Interplanetary Society*, Vol. 43, 1990, pp. 431–442.

[11]Fearn, D. G., "The Control Philosophy of the UK-10 and UK-25 Ion Thrusters," AIAA Paper 90-2629, July 1990.

[12]Harvey, M. S., et al., "The Advanced Propulsion Space Test Facilities at AEA Technology," 22nd International Electric Propulsion Conf., Culham Lab., Paper IEPC 91-153, Viareggio, Italy, Oct. 1991.

[13]Marchand, P., and Marmet, L., "Binomial Smoothing Filter: A Way to Avoid Some Pitfalls of Least-Squares Polynomial Smoothing," *Review of Scientific Instruments*, Vol. 54, No. 8, 1983, pp. 1034–1041.

[14]Jahn, R., *Physics of Electric Propulsion*, McGraw–Hill, New York, 1968 (Eqs. 4–16); also Spitzer, L., Jr., *Physics of Fully Ionized Gases*, Interscience, New York, 1956 (Eqs. 5–26).

[15]Bernstein, W., and Sellen, J. M., Jr., "Oscillations in Synthetic Plasma Beams," *Physics of Fluids*, Vol. 6, No. 7, 1963, pp. 1032, 1033.

[16]King, R. F., and Latimer, C. J., "The Formation of Fast Metastable and Ground-State Xenon Atoms by Electron Capture," *Journal of Physics B: Atomic and Molecular Physics*, Vol. 16, No. 4, 1983, pp. 583–590.

[17]Wadhwa, R. P., and Kooyers, G., "Analysis of Electron-Ion Mixing in Ion Engines," NASA CR-54033, March 1964.